Physics and Chemistry of the Earth 137 (2025) 103815

Contents lists available at ScienceDirect

Physics and Chemistry of the Earth

journal homepage: www.elsevier.com/locate/pce

Adsorption of hexavalent chromium from wastewater using magnetic biochar derived from peanut hulls

Lehlogonolo Tabana *, Annita Kupa, Shepherd Tichapondwa

Department of Chemical Engineering, Sustainable Environmental and Water Utilisation Processes Division, University of Pretoria, Pretoria, 0028, South Africa

ARTICLE INFO

Keywords:
Response surface methodology
Magnetic properties
Biomass
Pyrolysis
Adsorption efficiency

ABSTRACT

In this study, the utilization of peanut hulls as a precursor for the preparation of magnetic biochar through pyrolysis was investigated. To enhance the magnetic and adsorption properties of the biochar, the peanut hulls biomass was modified using ferric chloride hexahydrate and magnesium chloride hexahydrate. Response surface methodology was employed to evaluate the influence of biomass metal concentration, pyrolysis temperature, pyrolysis period and flow of nitrogen on the yield and Cr (VI) adsorption efficiency of the synthesized biochar. A 17-run experimental matrix was generated using Optimal Design to investigate the interactions among four input parameters. The results led to the development of a quadratic model, which demonstrated a high degree of predictability in accordance with the experimental data. Analysis of variance (ANOVA) confirmed that the models for yield and Cr (VI) adsorption efficiency were highly significant ($p < 0.05$), with coefficients of determination (R^2) values of 0.891 and 0.988, respectively. The optimal synthesis conditions for producing biochar with superior physicochemical properties were identified as a pyrolysis temperature of 300 °C, a pyrolysis duration of 2 h, a metal-to-biomass ratio of 0.5, and a constant flow of nitrogen. A desirability of 85% was achieved through numerical optimization, corresponding to a yield of 63% and complete Cr (VI) removal. Further optimization of Cr (VI) adsorption efficiency, considering the effects of pH (3–12), adsorbent loading (1–15 g/L), and initial Cr (VI) concentration (5–20 mg/L), was performed using a 19-run experimental matrix. ANOVA for Cr (VI) adsorption efficiency model revealed high significance ($p < 0.05$) with an R^2 value of 0.916.

The magnetic biochar demonstrated a remarkable adsorption efficiency of 98% under the experimental conditions of solution pH 3, adsorbent dosage of 5 g/L, and an initial Cr (VI) concentration of 20 mg/L. The desirability of 100% was obtained by a numerical optimization method representing Cr (VI) removal of 98%. The adsorption behaviour was adequately described by the Freundlich isotherm model, suggesting multilayer adsorption, with a maximum adsorption capacity of 12 mg/g. Biochar also proved to have strong magnetic properties which enhanced solid-liquid separation post adsorption experiments.

1. Introduction

Chromium, an environmental pollutant known for its high carcinogenic and toxic properties, is frequently detected in wastewater. Its main sources can be attributed to various industrial activities including tanning, electroplating, printing, and dyeing (Rodrigues et al., 2019). There are two stable forms of chromium that can be found in aqueous environments: trivalent chromium (Cr (III)) and hexavalent chromium (Cr (VI)). These forms interconvert depending on pH (Liang et al., 2020). Cr (VI) is a cause for concern because even at low concentrations, it has been shown to have harmful effects on human health. Adverse health outcomes, such as cancer, neurological disorders, bleeding, and damage to the kidneys and liver, are associated with its strong oxidizing capacity and ability to penetrate biological membranes (Xu et al., 2018; Kolomaznik et al., 2008). According to World Health Organization (WHO) guidelines, the concentration of Cr (VI) in water should not be higher than 50 μg/L to guarantee safe drinking water (World Health Organization, 2011). Moreover, 0.1 mg/L and 0.05 mg/L, respectively, are the allowable limits for releasing Cr (VI) into inland surface water and potable water (World Health Organization, 2000).

Several treatment techniques have been utilized for the remediation of wastewater containing chromium, including electrochemical processes, filtration, reverse osmosis, ion exchange, chemical precipitation, adsorption, and membrane separation (van Tran et al., 2019, 2020).

* Corresponding author.
E-mail address: tabana.ls@tuks.co.za (L. Tabana).

https://doi.org/10.1016/j.pce.2024.103815
Received 11 March 2024; Received in revised form 9 September 2024; Accepted 15 November 2024
Available online 16 November 2024
1474-7065/© 2024 The Author(s). Published by Elsevier Ltd. This is an open access article under the CC BY-NC license (http://creativecommons.org/licenses/by-nc/4.0/).

Adsorption is one of these techniques that has drawn a lot of interest as a potential strategy for the removal of inorganic pollutants, particularly heavy metals, because of its high efficiency, cost-effectiveness, and ecological sustainability. Adsorbents, including activated carbons, clays, and zeolites, have exhibited significant effectiveness in the removal of Cr (VI) from industrial wastewater owing to their efficient adsorption characteristics (Mohan and Pittman Jr, 2006). The unique chemical and physical characteristics of carbon-based adsorbents have led to their recognition as the preferred choice for water treatment applications (Santhosh et al., 2020). However, the practical application of carbon-based adsorbents, such as activated carbon with high sorption capacity, is limited by their high costs and time-consuming synthesis procedures (Daneshvar et al., 2017). Consequently, there has been a growing interest among researchers to develop low-cost adsorbents that can be utilized effectively in the adsorption process.

Biochar is a carbon-based material that is produced through the thermal decomposition of biomass in an environment with limited oxygen or in anaerobic conditions at temperatures exceeding 250 °C. It has been proven as a highly effective and economically viable adsorbent for the removal of heavy metals from water. It provides a viable alternative to expensive activated carbon for the treatment of heavy metal pollutants in wastewater. Biochar's inherent properties, such as its high porosity, physiochemical stability in water, and abundance of precursor materials, make it a viable option for water remediation (Santhosh et al., 2020). Several modifications have been investigated to improve the adsorption capacity of conventional biochar. These modifications include adding organic compounds with functional groups (Ma et al., 2014), blending metals, oxides, or ions (Zhang et al., 2012), and mixing with reducing or oxidizing salts (Pan et al., 2014). While traditional biochar is effective at pollutant removal, the challenge is in separating the biochar adsorbent powder from the treated water solution, as residual powder can potentially cause secondary pollution in water (Santhosh et al., 2020). Magnetization offers a viable solution to this concern, as the resulting magnetized biochar has strong paramagnetic and high saturation properties, allowing for the separation of solids and liquids (Tran et al., 2019). For example, Han et al. (2016) used peanut hulls to create a magnetic biochar modified with iron chloride and then conducted desorption experiments by decanting the supernatant and separating the magnetic biochar with a magnet.

The aim of this study was to assess the efficacy of magnetic biochar in the remediation of Cr (VI) from wastewater. The biochar was produced using the pyrolysis method, utilizing peanut hulls as the primary material, and modifying reagents such as magnesium chloride and ferric chloride. The removal efficiency was evaluated through batch adsorption experiments, which were conducted under different pH conditions, adsorbent dosages, and initial concentrations of Cr (VI). The objectives of the study were to synthesize and characterize magnetic biochar, optimize synthesis conditions through adsorption test runs, determine optimal adsorption conditions, explore adsorption kinetics and relevant isotherms for Cr (VI) removal, and assess the biochar's magnetic property using a magnet.

2. Experimental

2.1. Materials

Peanut hulls were obtained from small-scale farmers in Tzaneen, Limpopo Province. Ferric chloride hexahydrate ($FeCl_3{\cdot}6H_2O$) and magnesium chloride hexahydrate ($MgCl_2{\cdot}6H_2O$) from Glassworld (Pty) Ltd., South Africa, were used to improve the magnetic and adsorption properties of the produced biochar. Afrox provided the nitrogen gas (N_2) used in the biochar production. Potassium dichromate ($K_2Cr_2O_7$) from Merck (Pty) Ltd. was used to prepare synthetic solutions of Cr (VI). Hydrochloric acid (HCl) in a 32% solution was supplied by Sigma Aldrich, whereas solid sodium hydroxide (NaOH) was acquired from Merck (Pty) Ltd, both materials were used for pH adjustments. Deionized water from a Purelab Flex 3 water dispenser was used for dilutions and solution compositions.

2.2. Synthesis of magnetic biochar

A series of sequential preparatory steps were conducted on the peanut hulls. This included initial washing with deionized water to eliminate impurities (mainly soil), followed by crushing using a blender, and subsequent drying at 60 °C for 24 h in an oven. The crushed hulls underwent further pulverization to enhance the overall surface area. The experimental design for biochar synthesis was executed using Design Expert software (version 13.0, Stat-Ease Minneapolis, USA), considering four main operating parameters: pyrolysis temperature (A), ratio of metal salts to biomass (B), pyrolysis time (C), and the flow of N_2 (D). These parameters were systematically varied within specified ranges, pyrolysis temperature (200–600 °C), ratio of metal salts to biomass (ranging from 0 to 1 with increments of 0.25), pyrolysis time (1–6 h), and a categorical factor representing the flow of N_2 at 10 mL/min into the furnace. The Optimal Design approach was chosen because it allows for any type of input (numeric, discrete, or categorical) and accommodates any constraints while minimizing the number of experimental runs required for the specified polynomial model. This resulted in the formulation of a design matrix comprising 17 experimental test runs, as detailed in Table 1.

Biomass was modified by impregnation with a solution containing $FeCl_3{\cdot}6H_2O$ and $MgCl_2{\cdot}6H_2O$ at a Fe/Mg ratio of 1. The impregnation was done at a total solid to water ratio of 0.3:0.7, and the resulting mixture was agitated for 2 h using an overhead stirrer. The mixture was then filtered and dried in an oven for 24 h at 50 °C. The heat treatment parameters for both the modified biomass intended for magnetic biochar production and the unmodified biomass used in regular biochar production were as shown in Table 1.

2.3. Characterization

X-ray powder diffraction (XRD) analysis was conducted using a PANalytical X'Pert Pro powder diffractometer in θ-θ configuration, equipped with an X'Celerator detector and Co-Kα radiation with Fe-filtering. XRD spectra were collected in the angular range of 5–90° 2θ with a step size of 0.008° 2θ and a scan step time of 13 s. The mineral phases were identified using X'Pert Highscore plus software, which indexed the spectra against the ICSD database. For imaging the morphology, a Zeiss Ultra Plus field emission scanning electron

Table 1
Biochar synthesis experimental design matrix and results.

Run	Parameters				Responses	
	Pyrolysis temperature (°C)	Ratio of metal salts to biomass	Pyrolysis time (h)	Flow of nitrogen	Yield (%)	Cr(VI) removal (%)
1	600	1	1	no	25.40	68.04
2	400	1	3.5	no	26.80	100
3	600	0.5	1	yes	21.3	82.92
4	200	0	3.5	no	30.80	32.78
5	200	1	6	yes	70.89	49.36
6	600	1	1	yes	23.77	77.38
7	200	0	1	yes	66.82	38.42
8	400	0.5	3.5	yes	29.99	100
9	600	1	6	yes	15.48	50.14
10	200	1	6	no	65.75	90.68
11	200	0.5	1	no	59.04	98.38
12	200	1	1	yes	52.09	100
13	200	0	6	yes	40.95	74.74
14	200	0	1	yes	55.34	43.42
15	300	0.5	4.75	no	44.20	100
16	400	0.25	2.25	no	34.19	100
17	200	0	3.5	no	58.05	51.04

microscope (FEG-SEM) was utilized. Samples were prepared by distributing them on carbon tape affixed to a microscopy stub, followed by carbon sputter coating under argon gas. The BET surface area was determined using a Micrometrics Tristar 3000 BET analyzer. Before analysis, the samples were degassed for 24 h at 150 °C under a 10^{-5} Torr vacuum. Identification of the main functional groups and anions in the samples was done on a PerkinElmer 100 Spectrophotometer. The instrument was equipped with a MIRacle attenuated total reflection (ATR) attachment which had a zinc-selenide (ZnSe) crystal plate. A powdered sample weighing ca. 20 mg was placed onto the crystal plate and pressed by lowering down the pressure arm until the force gauge was ca. 80 before data could be collected. The spectra were recorded between 550 and 4000 cm^{-1} at a resolution of 2 cm^{-1} with data collected over 32 scans. An Eriez Magna Chute BaFe, with a magnetic intensity of 1370 Gauss, was utilized to separate the magnetic and non-magnetic components of the biochar. The process commenced by pouring the sample onto a flat tray in contact with the magnet. The sample was then rinsed with water to remove the non-magnetic components. Subsequently, the tray was raised above the magnet, allowing the magnetic portion to fall to the back for collection. The slurries containing both the magnetic and non-magnetic samples were filtered, dried, and weighed. This procedure was repeated three times to ensure reliability, accuracy, and repeatability.

2.4. Batch adsorption studies

2.4.1. Determining the optimal conditions for biochar synthesis

The optimal conditions for biochar synthesis were evaluated using two key indicators: percentage yield (*P*) and Cr(IV) removal efficiency (*R*). Percentage yield was calculated by taking the ratio of the final weight (W_f) after thermal treatment to the initial weight (W_i) before treatment, as indicated in Equation (1). Removal efficiency was determined through adsorption tests using the residual biochar, as shown in Equation (2). An appropriate volume of deionized water was used to diluted a 1000 mg/L stock solution in order to produce aqueous solutions of Cr(VI) with an initial concentration of 5 mg/L. Batches of 1 g biochar were added into separate 100 mL portions of the 5 mg/L Cr(VI) solutions. A shaker was utilized to agitate these mixtures for a duration of 24 h at room temperature, with the speed set at 200 rpm. A total of 17 experimental runs were carried out, and the resulting samples were filtered using 0.45 μm syringe filters prior to analysis. The PerkinElmer Analyst 400 Atomic Absorption Spectrophotometer (AAS) was used for the residual analysis of Cr (VI).

$$P = \frac{W_f}{W_i} \times 100 \quad (1)$$

$$R = \frac{(C_0 - C_t)}{C_0} \times 100 \quad (2)$$

Where C_0 and C_t represent the initial concentration of Cr (VI) and the concentration at any given time (t) respectively.

2.4.2. Optimization of Cr (VI) adsorption tests

A thorough investigation was conducted to determine the optimal adsorption conditions by evaluating the effects of initial pH of the solution (*E*), adsorbent loading (*F*), and the initial Cr (VI) concentration (*G*) on the adsorption efficiency. The biochar synthesized under the optimal conditions outlined in Section 2.4.1 was utilized for this purpose. The initial Cr (VI) concentration was varied from 5 to 20 mg/L, while the initial pH ranged from 3 to 12 with the adsorbent loading varying from 1 to 15 g/l. A total of 19 experimental runs were conducted in accordance with the simulated design matrix provided by Stat-Ease as shown in Table 2. Further tests were conducted to investigate the adsorption kinetics, isotherms and the adsorbent's stability and reusability.

Table 2
Adsorption experimental design matrix and results.

Run	Parameters			Response
	pH	Adsorbent loading (g/L)	Pollutant concentration (mg/L)	Cr (VI) removal (%)
1	12	1	5	1.59
2	5	5	10	98.19
3	3	15	10	97.29
4	7	1	15	87.87
5	3	10	5	93.30
6	7	10	15	96.86
7	9	15	10	98.70
8	12	15	5	98.80
9	3	5	20	97.16
10	9	5	10	99.41
11	3	1	5	79.91
12	7	10	5	98.89
13	12	1	20	0.38
14	5	15	20	97.87
15	7	10	5	98.67
16	12	10	15	98.78
17	12	15	20	99.50
18	7	1	15	60.37
19	12	10	15	99.23

3. Results and discussion

3.1. Characterization of neat and modified peanut hulls

3.1.1. X-ray diffraction

Fig. 1 depicts the X-ray diffraction (XRD) patterns for both the neat and processed biomass. Notably, peaks at 2θ = 18.21° and 25.62°, corresponding to d-spacing values of 0.57 nm and 0.4 nm, respectively, appear in both the unmodified and metallized biomass. The identification of these peaks strongly supports the presence of cellulose within the biomass matrix (Silva et al., 2020). The peaks are absent from the XRD pattern of the magnetic biochar which indicates that the material underwent a significant transformation during the pyrolysis process. This transformation denotes a change from crystalline to amorphous, which improves the adsorption capacity of the resultant material (Zhong et al., 2012).

3.1.2. Scanning electron microscopy (SEM) and BET surface area analysis

Fig. 2 presents scanning electron microscopy (SEM) images of distinct biomasses: neat peanut hull (a), metallized peanut hull (b), and

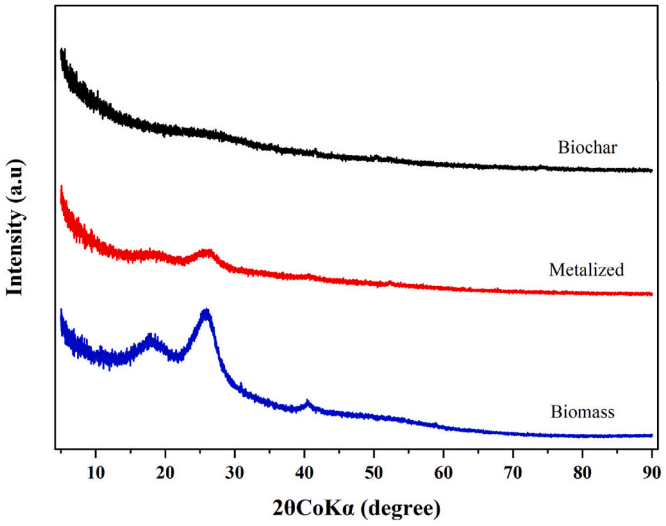

Fig. 1. X-ray diffraction spectra for pristine peanut hulls biomass, metallized biomass, and magnetic biochar.

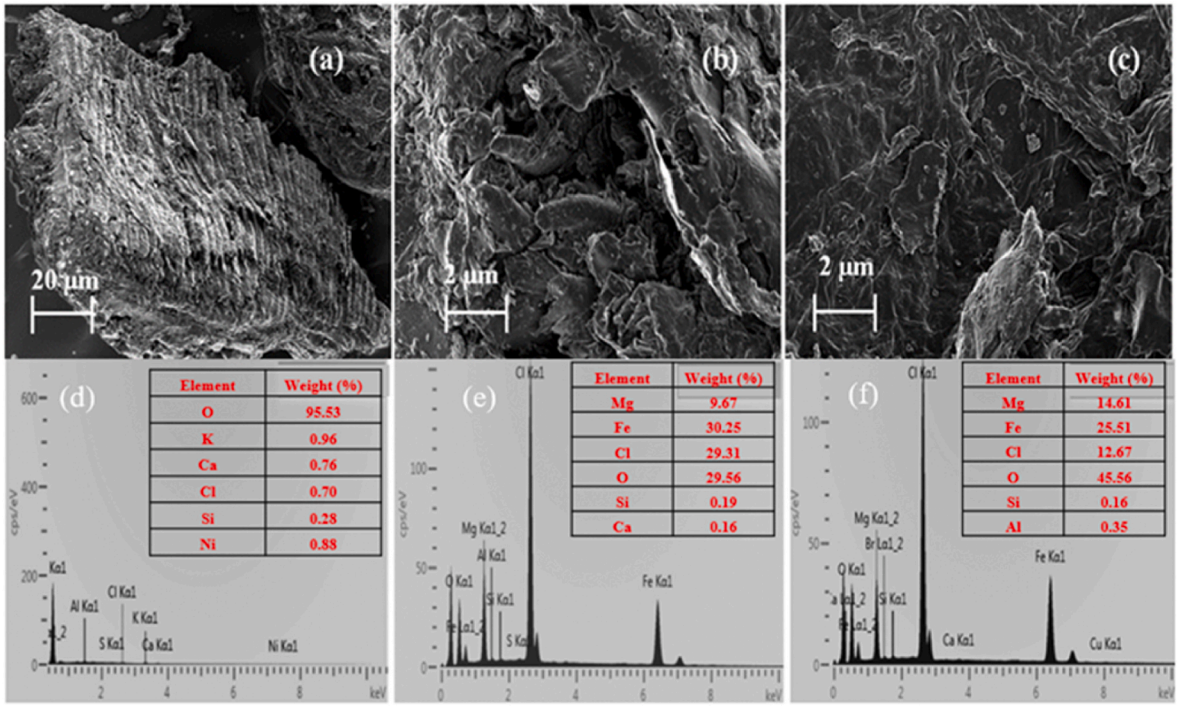

Fig. 2. SEM images and SEM/EDS analysis for Pristine peanut hulls biomass (a) and (d), Metallized peanut hulls biomass (b) and (e), and Magnetic biochar (c) and (f).

magnetic biochar (c). SEM images of neat peanut hulls display a fibrous and porous texture which is a characteristic of cellulose-containing materials (Zhong et al., 2012). In the metallized biomass sample, sheet-like structures are observed, and the rod-like texture is not evident due to the presence of added metal salts. Upon thermal treatment at 300 °C, the metallized biomass underwent transformation into magnetic biochar, exhibiting an irregular shape with micro and mesopores. Additionally, SEM images of the magnetic biochar reveal the presence of small particles on its surface, attributed to the metal oxides (Fe and Mg) incorporated during the metallization process. The elemental compositions of the neat biomass, metallized biomass, and magnetic biochar, as determined through energy dispersive X-ray spectroscopy (EDS), are presented in Fig. 2(d)–(f). Carbon was not quantified in this study because the materials used to prepare the samples for SEM/EDS analysis contained carbon. As a result, the carbon content measured would not provide an accurate representation of the actual carbon present in the samples. The metallized biomass and magnetic biochar both exhibited the presence of Mg and Fe, confirming the successful impregnation of the biomass with metal salts. However, after the thermal treatment of the metallized biomass to produce magnetic biochar, a decline in the observed metallic composition was noted, likely due to partial volatilization during the thermal process. The BET surface area for the neat peanut hulls, metallized peanut hulls and magnetic biochar were established to be 6.42, 3.63 and 24.29 m^2/g. The reduction in surface area observed when neat peanut hulls are mixed with metal salts can be ascribed to the adsorption of chloride ions by the active sites present on the neat peanut hulls. Conversely, the augmentation in surface area following thermal treatment can be attributed to the generation of metal oxides and the concurrent development of pores in the resulting biochar. The BET surface area hysteresis, depicted in Fig. S1 (in the supplementary section), exhibits a Type V isotherm, as categorized by IUPAC. This type of isotherm is commonly associated with porous adsorbents and indicates weak interactions between the adsorbate and adsorbent (Nnadozie and Ajibade, 2020). The pore distribution plots, shown in the inset of Fig. S1, reveal a mesoporous structure, with an average pore size ranging from 20 to 25 nm for the adsorbents.

3.1.3. *Fourier-transform infrared spectroscopy (FTIR)*

Fig. 3 depicts the Fourier-transform infrared (FTIR) spectra for neat peanut hulls, metallized biomass, and biochar. No significant differences were observed between the neat and metallized biomass materials. The peak at 1569 cm^{-1} is attributed to C–C, C–H, or C–O stretching vibrations, while the peak at 1024 cm^{-1} is associated with the C–O group in carboxylic and alcoholic groups (Ossman et al). The slightly broad peak at 1560 cm^{-1} is ascribed to C═C stretching vibrations due to aromatic and carboxylic compounds (El-Hendawy, 2006), and the signals observed at 1268, 1186, and 1033 cm^{-1} are attributed to C–H stretching vibrations from aromatic compounds with angular deformation in the plane (Raj et al., 2009). In both spectra, the broad band at 3345 cm^{-1} is associated with the O–H stretch from the carboxylic group (El-Hendawy, 2006). In the magnetic biochar spectrum, the broad peak with a

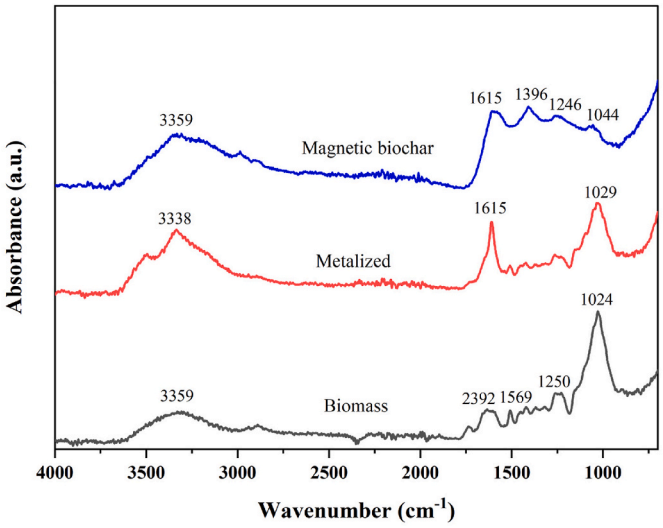

Fig. 3. FTIR analysis for neat biomass, metallized biomass and magnetic biochar.

maximum value of 3388 cm^{-1} is associated with the stretching vibrations of O–H (Liu et al., 2010). The peak at 2921 cm^{-1} is attributed to the C–H stretching of methyl and methylene groups found in the lignocellulosic constituents (Picard et al., 2020).

3.2. Magnetic biochar synthesis

3.2.1. Model fitting and statistical analysis

Table 1 presents a comprehensive design matrix with corresponding responses. Biochar yield (Y_1) ranged from 16 to 71% while Cr (VI) adsorption efficiencies (Y_2) varied between 38 and 100%. The operational parameters A, B, C, and D for Y_1 and Y_2 were subjected to an analysis of model fit summary and analysis of variance (ANOVA) to assess the adequacy of the empirical models. These models are expressed by Equations (3) and (4), respectively. The models for yield and Cr (VI) adsorption efficiency were found to be highly significant ($p < 0.05$), with coefficients of determination (R^2) of 0.891 and 0.988, respectively. Detailed ANOVA results for yield and adsorption efficiencies are presented in Tables 3 and 4 respectively. Notably, the models' F-values for yield and adsorption efficiencies were 32.52 and 16.65. These F-values indicate statistical significance, with a minimal probability (0.01%) that larger F-values could have arisen from random noise. Furthermore, the p-values for each model term listed in Tables 3 and 4 were below 0.05, indicating their statistical significance. Fig. 4 (a) and (b) present the actual versus predicted response values for yield and Cr (VI) adsorption efficiency, respectively. The close alignment of the actual and predicted experimental values with the straight lines indicates a strong correlation between the observed and predicted results.

$$Y_1 = 25.68 - 20.70A + 7.67B - 3.66C - 16.07AB + 5.35BC + 9.56A^2 \quad (3)$$

$$Y_2 = 106.23 + 1.99A + 33.49B - 14.59C + 16.07D - 15.50AB + 10.90AC - 35.60A^2 - 46.86B^2 \quad (4)$$

3.2.2. Biochar yield

Fig. 5 depicts a three-dimensional response surface and contour plots that show the interactions between metal salts to biomass ratio and pyrolysis time, and metal salts to biomass ratio with pyrolysis temperature. Nitrogen flow was found to be insignificant in influencing yield. Fig. 5 clearly shows that using metallized biomass with a metal salt to biomass ratio greater than 0.5, combined with a thermal treatment duration of less than 3 h, resulted in a higher biochar yield. Conversely, as anticipated, higher temperatures led to decreased yields.

3.2.3. Chromium adsorption

Fig. 6(a)–(d) depict three-dimensional response surfaces and contour plots that demonstrate the Cr (VI) adsorption efficiencies of biochar produced under varying pyrolysis time, temperature, and metal salts to biomass ratio conditions. An evident pattern is the decline in biochar adsorption efficiency with increasing pyrolysis temperature and duration. The decline in adsorption efficiency can be ascribed to the altered composition of the biochar resulting from treatment at elevated temperatures for prolonged durations. At this stage, the material was predominantly composed of ash components. Conversely, as depicted in Fig. 6(a), biochar derived from metallized biomass, employing a range of metal salts to biomass ratios from 0.5 to 1 and undergoing pyrolysis at intermediate temperatures between 200 and 400 °C, exhibited favourable efficiencies in the adsorption of Cr (VI). The optimal pyrolysis conditions were set at 300 °C for 2 h with a metal salt to biomass ratio of 0.5 and a continuous flow of N_2.

Table 3
ANOVA assessed the quadratic response surface model for synthesis of biochar (based on yield).

Source	Sum of squares	DF	Mean square	F-value	P-value
Model	10188.63	4	2547.16	32.52	<0.0001
A-Temperature	8464.12	1	8464.12	83.38	<0.0001
B-Metal salts to biomass ratio	1165.68	1	1165.68	11.48	0.0031
C-Pyrolysis time	371.46	1	371.46	3.66	0.0709
AB	346.05	1	346.05	10.56	0.04
BC	154.66	1	154.66	3.51	0.0011
A^2	116.45	1	116.45	4.56	0.0022
Residual	1928.66	19	101.51		
Lack of fit	1491.15	14	106.51	1.22	0.4455
Pure error	437.5	5	87.50		

Table 4
ANOVA assessed the quadratic response surface model for synthesis of biochar (based on removal efficiency).

Source	Sum of squares	DF	Mean square	F-value	P-value
Model	8946.52	6	1652.26	16.65	<0.001
A-Temperature	6874.53	1	6874.52	78.54	0.0025
B-Metal salts to biomass ratio	984.63	1	984.24	13.85	0.0031
C-Pyrolysis time	286.63	1	286.63	7.68	0.032
D-Flow of nitrogen	124.55	1	124.55	8.66	0.052
AB	289.66	1	289.66	9.89	0.042
AC	174.36	1	174.36	6.55	0.048
A^2	119.78	1	119.78	5.53	0.051
B^2	85.89	1	85.89	6.78	0.042
Residual	1678.34	18	97.51		
Lack of fit	1156.59	14	107.51	2.56	0.6891
Pure error	521.75	4	92.50		

3.2.4. Numerical optimization for biochar synthesis

To optimize the synthesis of biochar, a numerical optimization process was carried out using Design-Expert software. The factors were varied within specified ranges: pyrolysis temperature (200–600 °C), metal salts to biomass ratio (0–1), pyrolysis duration (1–6 h), and nitrogen flow (Yes or No). The response variables, which included yield and adsorption efficiency, were optimized at a 95% confidence level. The desirability function approach was utilized, with the optimized conditions illustrated in Fig. 6. Out of the 49 possible solution configurations, the most favourable (85%) and optimal condition, depicted in Fig. 7, was identified with a pyrolysis temperature of 300 °C, a metal salts to biomass ratio of 0.5, a pyrolysis time of 2 h, and a continuous flow of nitrogen. Some of the optimal conditions along with their corresponding desirability values are presented in Table S1. The experimentally validated optimum conditions were in close agreement with the predicted values, showing deviations of less than 5%.

3.3. Adsorption optimization

3.3.1. Model fitting and statistical analysis

Table 2 presents the comprehensive design matrix, including the corresponding adsorption efficiency values obtained from the adsorption optimization studies. Cr (VI) adsorption efficiency ranged from 1.59 to 99.89%. By analyzing the sequential model sum of squares, the model with the highest order polynomial was selected, considering additional terms that were statistically significant. The chosen model for the Cr (VI) adsorption efficiency (Y_3) in terms of the adsorption condition factors *E, F,* and *G* was a quadratic model, represented by Equation (5). The quality of the model was assessed using the correlation coefficient (R^2), which yielded a value of 0.916. This indicates a strong agreement between the predicted response from the model and the experimental data. The R^2 value for the quadratic model was higher compared to other models considered, further supporting its suitability. This observation is further validated in Fig. 8, which contrasts the predicted values from the model with the experimental results. The linear trend observed in the data points suggests that the residuals are normally distributed,

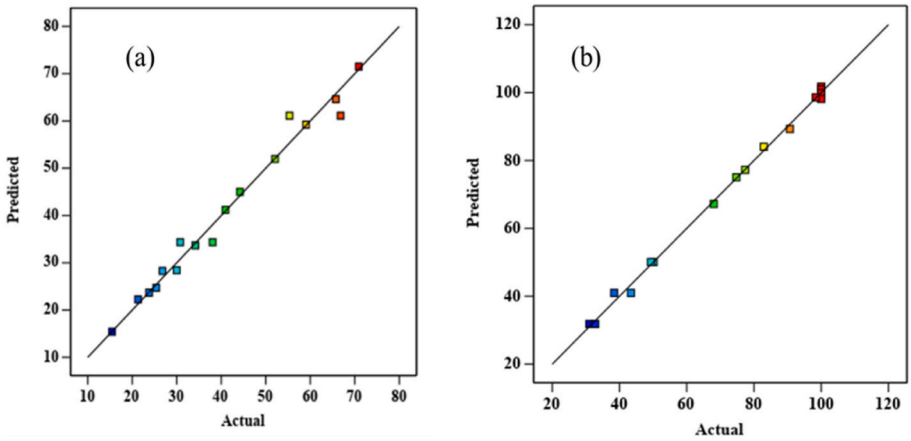

Fig. 4. Comparison between the predicted and actual responses (a) Yield and (b) Cr (VI) adsorption efficiency.

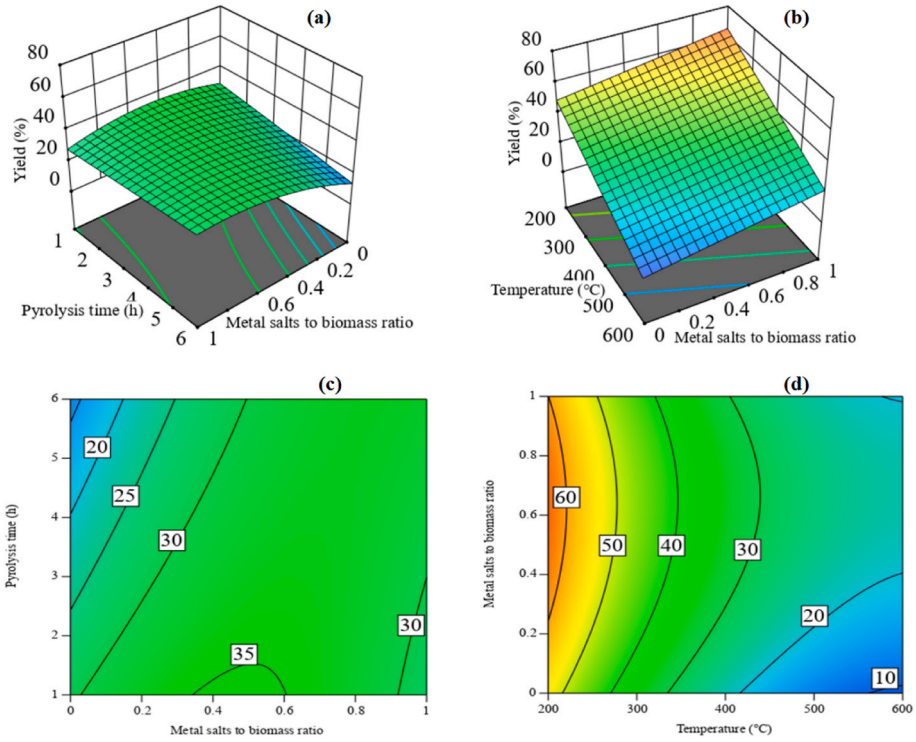

Fig. 5. 3D surface plots and contour plots of biochar yield: (a) and (c) effect of pyrolysis time and metal salts to biomass ratio; (b) and (d) effect of pyrolysis temperature and metal salts to biomass ratio.

eliminating the necessity for data transformation. Consequently, it can be concluded that the quadratic model's predictions for Cr (VI) adsorption by magnetic biochar are reasonably accurate and satisfactory. To validate the competency of the model, ANOVA was conducted, and the results are presented in Table 5. The interaction between the pH (E) of the solution and the adsorbent loading (F) was found to be statistically significant. The effect of pollutant concentration (G) was determined to be non-significant (p-value = 0.885). However, the term G was incorporated into the model to maintain hierarchical structure.

$$Y_3 = 105.49 - 15.23E - 21.98F + 0.43G + 23.26EF - 18.79F^2 - 18.62G^2 \quad (5)$$

3.3.2. *Effect of adsorbent loading and pH*

Fig. 9 presents the Cr (VI) adsorption efficiencies through 3D (a) and contour (b) plots, illustrating its dependence on both the initial pH of the solution and the adsorbent dosage. The results indicate distinct effects of pH and adsorbent loading on adsorption efficiency. A direct proportionality is observed between adsorbent loading and adsorption efficiency, attributed to increased availability of adsorption sites per unit of loaded adsorbent. With higher magnetic biochar loading, more adsorption sites become accessible, resulting in increased removal efficiency of Cr (VI). Conversely, a decrease in adsorption efficiency is noted with an increase in pH levels. In aqueous solutions, Cr (VI) exists in three primary speciation forms: $HCrO_4^-$, $Cr_2O_7^{2-}$, and CrO_4^{2-}, as illustrated in Fig. S2 in the supplementary materials. The latter is prevalent in solutions with a basic pH, while the first two are more prominent in acidic pH solutions. The point of zero charge for magnetic biochar is determined at a pH of 4, as shown in Fig. S3 in the supplementary data. This indicates that magnetic biochar exhibits the highest affinity for Cr (VI) and anions in solutions with pH levels below 4, primarily through electrostatic interactions, resulting in higher observed adsorption

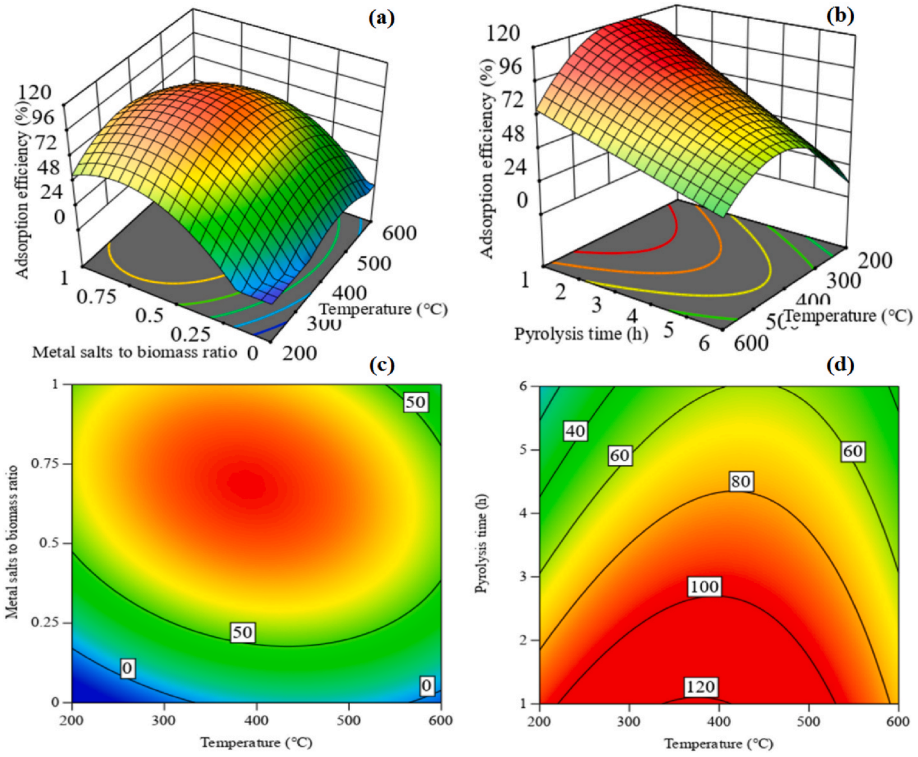

Fig. 6. 3D surface plots and contour plots of chromium adsorption efficiency: (a) and (c) effect of pyrolysis time and pyrolysis temperature; (b) and (d) effect of metal salts to biomass ratio and pyrolysis temperature.

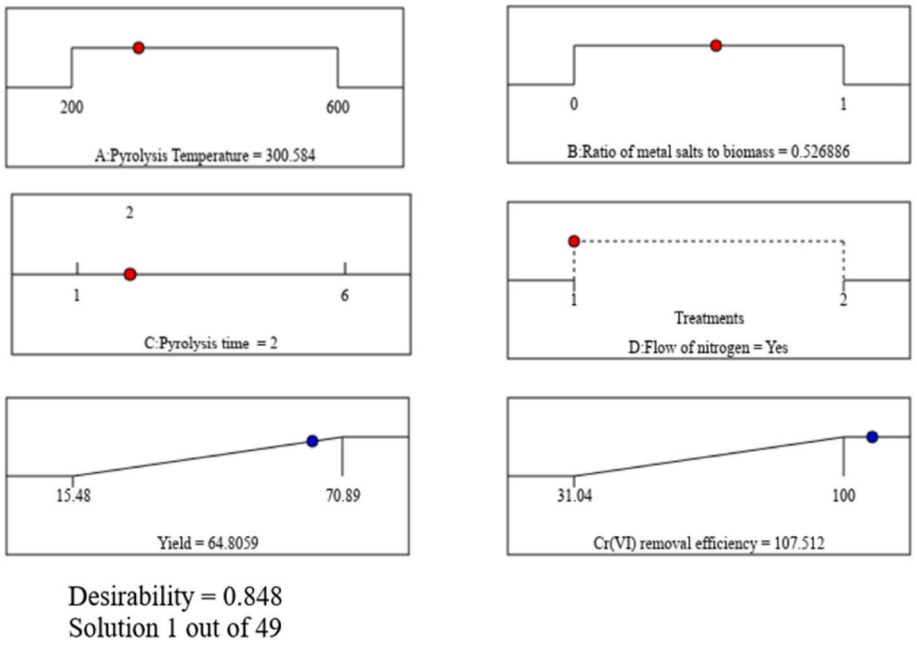

Fig. 7. Ramp plot of numerical optimized conditions with the desirability of 85%.

efficiencies in acidic solutions. The optimal conditions were identified at a pH value of 3 and an adsorbent loading of 5 g/L.

3.3.3. *Numerical optimization*

To improve the effectiveness of Cr (VI) removal, a numerical optimization process was carried out using Design-Expert software. The factor levels were adjusted within specified ranges: solution pH (3–12), adsorbent loading (1–15 g/L), and initial contaminant concentration (5–20 mg/L). The response variable, which was adsorption efficiency, was optimized with a 95% confidence level. The desirability function approach was applied, with the optimized conditions illustrated in Fig. 10. Among the 64 possible configurations, the most favourable (100%) and optimal condition, as shown in Fig. 10, was identified at a pH of 3, an adsorbent loading of 5 g/L, and an initial contaminant concentration of 20 mg/L. Additional optimal conditions and their corresponding desirability values are detailed in Table S2. The

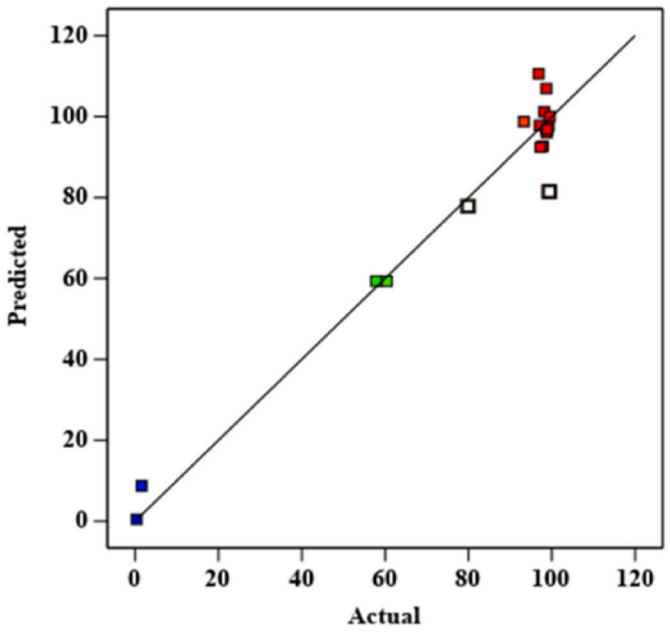

Fig. 8. Comparison between the predicted and actual Cr (VI) adsorption efficiency. responses.

Table 5
ANOVA assessed the quadratic response surface model for optimizing chromium adsorption efficiency.

Source	Sum of squares	DF	Mean square	F-value	P-value
Model	15689.09	5	3137.82	27.62	<0.0001
E	2441.47	1	2441.47	21.49	0.0005
F	5163.66	1	5163.66	45.45	<0.0001
G	1.83	1	1.83	0.022	0.885
EF	3624.03	1	3624.03	31.90	<0.0001
F^2	1252.94	1	1252.94	11.03	0.0055
G^2	1261.30	1	1261.30	11.10	0.0054
Residual	1477.10	13	113.62		
Lack of fit	1098.02	10	109.80	0.8690	0.624
Pure error	379.08	3	126.36		

experimentally validated optimum conditions closely matched the predicted values, with deviations of less than 5%.

3.4. Effect of contact time and adsorption kinetics

Fig. 11 depicts the effect of time on Cr (VI) adsorption by magnetic biochar, showcasing a rapid removal process that results in equilibrium being reached within 60 min. The amount of mass adsorbed at a given time was determined using Equation (6). Fig. 12 depict the fitting of the kinetics data onto the pseudo-first order (PFO) model as determined using Equation (7) (The plot for the pseudo-second order model is shown by Fig. S4). The kinetics data in Table 6 shows that the PFO model exhibits a commendable goodness of fit, as evidenced by a high R^2 value of 0.993. In contrast, the application of the pseudo-second order (PSO) model to the experimental dataset yields a diminished R^2 value of 0.916, indicating a comparatively suboptimal fit to the model.

$$q_t = \frac{V}{m}(C_0 - C_t) \tag{6}$$

$$q_t = q_e\left(1 - e^{-K_1 t}\right) \tag{7}$$

$$q_t = \frac{q_e^2 K_2 t}{q_e K_2 t + 1} \tag{8}$$

Where q_t is the adsorption capacity at time = t (mg/g); V is the volume of wastewater solution (L); m is the mass of adsorbent (g); K_1 is the first order rate constant (min^{-1}); K_2 is the second order rate constant (g/mg·min).

3.5. Adsorption isotherms

Fig. 13 depicts the experimental data fitted to the Langmuir and Freundlich equilibrium isotherm models. These models are represented by Equations (9) and (10) respectively. Table 7 shows the corresponding parameters for these fitted isotherm models. The Freundlich model provided a good fit with a maximum adsorption capacity of 12 mg/g. This finding shows that Cr (VI) adsorption involved chemical interactions, potentially caused by electrostatic interactions between the magnetic biochar and Cr(VI) ions.

$$q_e = K_F C_e^n \tag{9}$$

$$q_e = \frac{q_m K_L C_e}{1 + K_L C_e} \tag{10}$$

Where K_F is the Freundlich equilibrium constant (L/g); K_L is the Langmuir constant (L/mg); C_e is the pollutant concentration at equilibrium

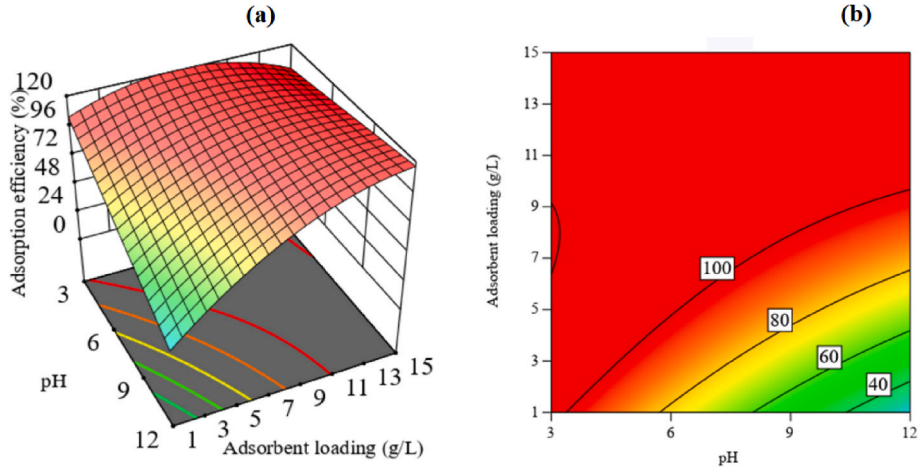

Fig. 9. 3D surface plot (a) and contour plot (b) of chromium adsorption efficiency: effect of pH of chromium solution and adsorbent loading.

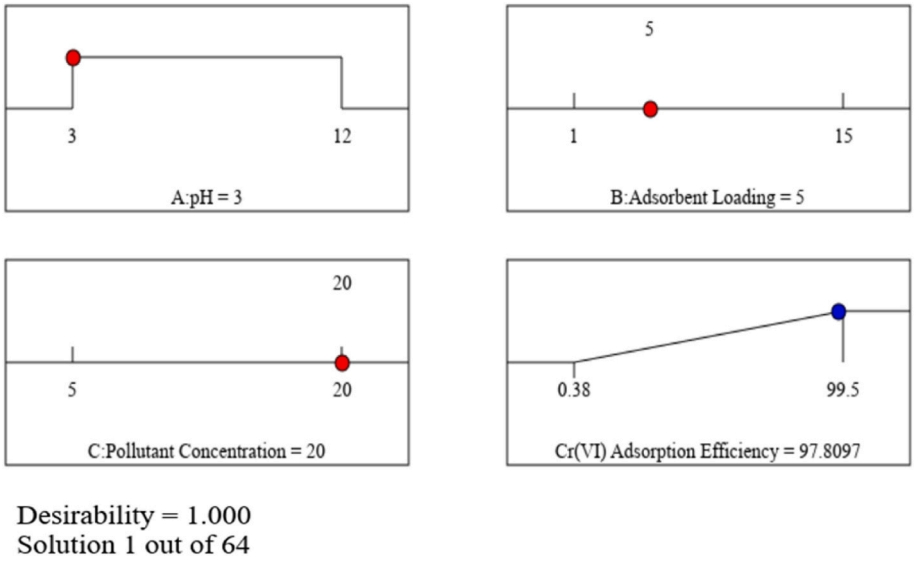

Fig. 10. Ramp plot of numerical optimized conditions with the desirability of 100%.

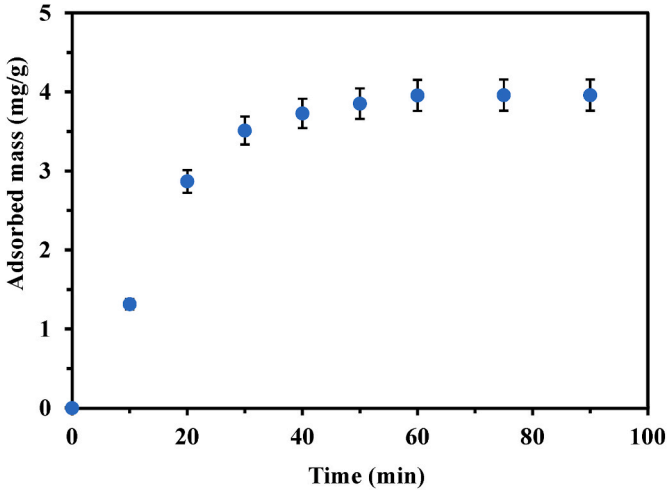

Fig. 11. Effect of time on amount of Cr(VI) adsorbed (pH 3, 20 mg/L and 5 g/L loading).

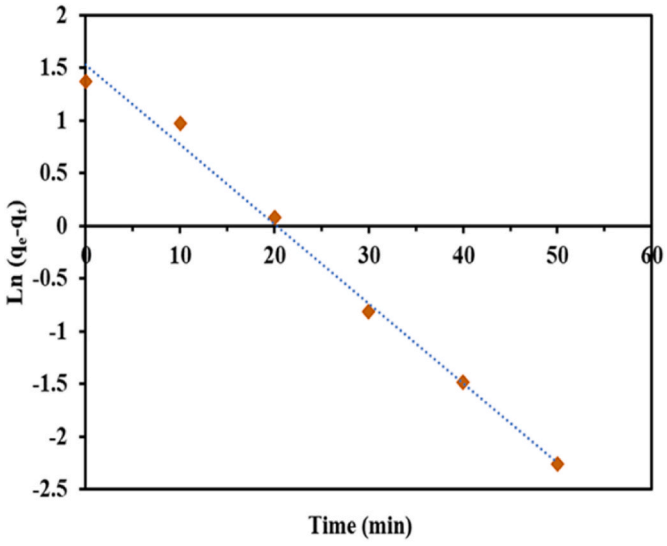

Fig. 12. Pseudo first order kinetic data fits using (pH 3, 20 mg/L and 5 g/L loading).

(mg/L); n is the heterogeneity constant (dimensionless); q_e is the mass adsorbed at equilibrium (mg/g); q_m is the maximum adsorption capacity (mg/g).

3.6. Adsorption mechanism, magnetism, and reusability studies

Chromate ion has various forms in solution such as CrO_4^{2-}, $HCrO_4^-$ and $Cr_2O_7^{2-}$ depending on the operating pH. Similarly, the surface charge of the adsorbent is also a function of pH hence the point of zero charge was established to be 4 as shown in Fig. S3 in the supplementary data. This means that the adsorbent was positively charged at the operation pH of 3. Concurrently, the dominant chromate species at pH 3 is CrO_4^{2-}. Based on the charges of both the adsorbate and adsorbent, the hypothesized adsorption mechanism is electrostatic interactions. This conforms with the adsorption isotherm results which showed that the adsorption process was chemisorption. The biochar's magnetic properties were verified through pre and post-adsorption tests using a magnetic bar as shown by Fig. S5 (in the supplementary section). The results show the successful removal of Cr (IV) from the solution, the settling strength of the biochar and its substantial magnetic characteristics, as indicated by the attraction of biochar particles to the magnetic bar. A confirmatory test for magnetism using the Magna Chute instrument revealed that approximately 60% of the biochar was magnetic, as detailed in Table S3 of the supplementary data. This indicates that a significant portion of the biochar has can be recovered as magnetic material post adsorption process thereby enhancing its reusability. Fig. 14 shows the Cr (VI) adsorption efficiencies following the regeneration and reuse of magnetic biochar. An appreciable reduction in adsorption efficiency, amounting to 16%, was evident after the fifth consecutive run. This decline is ascribed to a diminution in active surface sites resulting from successive interactions with aqueous solutions and thermal treatment. The consistent achievement of heightened adsorption efficiencies across the

Table 6
Parameters of the adsorption kinetics models fitted.

PFO			PSO		
K_1 (min^{-1})	q_e(mg/g)	R^2	K_2 (g/mg·min)	q_e(mg/g)	R^2
0.01	1.452	0.993	0.174	2.73	0.916

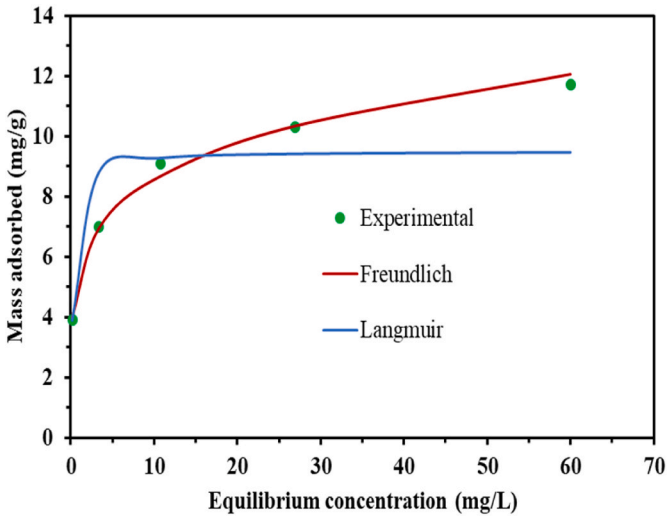

Fig. 13. Adsorption isotherm for Cr (VI) adsorption at pH 5, adsorbent loading of 5 g/L and 24 h contact time.

Table 7
Parameters of the isotherm models fitted.

Langmuir			Freundlich		
q_m (mg/g)	K_L	R^2	K_F	n	R^2
9.5	3.67	0.928	5.49	5.2	0.996

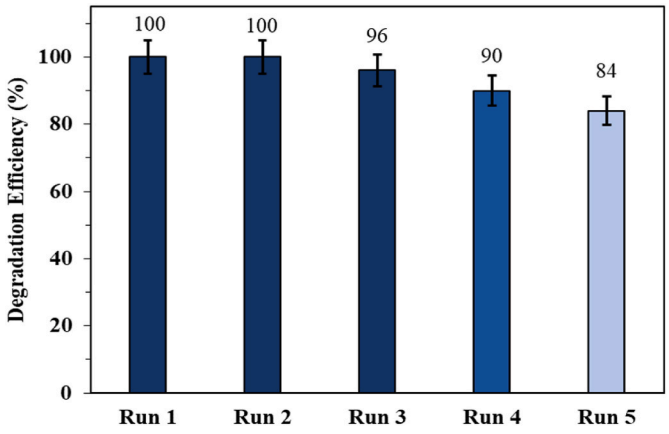

Fig. 14. Reusability studies for magnetic biochar (pH 3, 20 mg/L and 5 g/L loading).

initial four runs demonstrates the magnetic biochar's robust capability to adsorb heavy metals from wastewater.

4. Conclusion

In this study, peanut hulls were successfully utilized as a precursor for synthesizing magnetic biochar through pyrolysis. The biochar's magnetic and adsorption properties were enhanced using ferric chloride hexahydrate and magnesium chloride hexahydrate. Response surface methodology (RSM) was applied to investigate the influence of critical factors, including biomass metal concentration, pyrolysis temperature, pyrolysis duration, and nitrogen flow, on the yield and Cr (VI) adsorption efficiency. The development of a quadratic model demonstrated excellent predictive accuracy with high significance, yielding R^2 values of 0.891 and 0.988 for yield and Cr (VI) adsorption efficiency, respectively. The optimal synthesis conditions, including a pyrolysis temperature of 300 °C, a pyrolysis duration of 2 h, a metal-to-biomass ratio of 0.5, and nitrogen flow, resulted in a desirability of 85%, corresponding to a 63% yield and complete Cr (VI) removal. Additional optimization of Cr (VI) adsorption efficiency, accounting for pH, adsorbent loading, and initial Cr (VI) concentration, further demonstrated an adsorption efficiency of 98% at pH 3. The adsorption process was accurately described by the Freundlich isotherm, indicating multilayer adsorption, with a maximum adsorption capacity of 12 mg/g. The results reveal the potential for practical application of biochar derived from peanut hulls in water treatment, with strong magnetic properties facilitating efficient solid-liquid separation post-adsorption.

CRediT authorship contribution statement

Lehlogonolo Tabana: Writing – review & editing, Writing – original draft, Visualization, Investigation, Funding acquisition, Formal analysis, Data curation, Conceptualization. **Annita Kupa:** Writing – review & editing, Writing – original draft, Visualization, Investigation. **Shepherd Tichapondwa:** Writing – review & editing, Supervision, Resources, Funding acquisition.

Declaration of competing interest

The authors declare that they have no known competing financial interests or personal relationships that could have appeared to influence the work reported in this paper.

Acknowledgement

The authors are grateful for the financial support from the National Research Foundation (NRF) of South Africa (grant numbers:117905 and MND200409512185).

Appendix A. Supplementary data

Supplementary data to this article can be found online at https://doi.org/10.1016/j.pce.2024.103815.

Data availability

Data will be made available on request.

References

Daneshvar, E., Vazirzadeh, A., Niazi, A., Sillanpää, M., Bhatnagar, A., 2017. A comparative study of methylene blue biosorption using different modified brown, red and green macroalgae–Effect of pretreatment. Chem. Eng. J. 307, 435–446. https://doi.org/10.1016/j.cej.2016.08.093.

El-Hendawy, A.N.A., 2006. Variation in the FTIR spectra of a biomass under impregnation, carbonization and oxidation conditions. J. Anal. Appl. Pyrolysis 75, 159–166. https://doi.org/10.1016/j.jaap.2005.05.004.

Han, Y., Cao, X., Ouyang, X., Sohi, S.P., Chen, J., 2016. Adsorption kinetics of magnetic biochar derived from peanut hull on removal of Cr (VI) from aqueous solution: effects of production conditions and particle size. Chemosphere 145, 336–341. https://doi.org/10.1016/j.chemosphere.2015.11.050.

Kolomaznik, K., Adamek, M., Andel, I., Uhlirova, M., 2008. Leather waste – potential threat to human health, and a new technology of its treatment. J. Hazard Mater. 160, 514–520. https://doi.org/10.1016/j.jhazmat.2008.03.070.

Liang, M., Ding, Y., Zhang, Q., Wang, D., Li, H., Lu, L., 2020. Removal of aqueous Cr (VI) by magnetic biochar derived from bagasse. Sci. Rep. 10, 1–13. https://doi.org/10.1038/s41598-020-78142-3.

Liu, Y., Sun, X., Li, B., 2010. Adsorption of Hg^{2+} and Cd^{2+} by ethylenediamine modified peanut shells. Carbohydr. Polym. 81, 335. https://doi.org/10.1016/j.carbpol.2010.02.020, 33.

Ma, Y., Liu, W.J., Zhang, N., Li, Y.S., Jiang, H., Sheng, G.P., 2014. Polyethylenimine modified biochar adsorbent for hexavalent chromium removal from the aqueous solution. Bioresour. Technol. 169, 403–408. https://doi.org/10.1016/j.biortech.2014.07.014.

Mohan, D., Pittman Jr, C.U., 2006. Activated carbons and low-cost adsorbents for remediation of tri-and hexavalent chromium from water. J. Hazard Mater. 137, 762–811. https://doi.org/10.1016/j.jhazmat.2006.06.060.

Nnadozie, E.C., Ajibade, P.A., 2020. Adsorption, kinetic and mechanistic studies of Pb (II) and Cr (VI) ions using APTES functionalized magnetic biochar. Microporous Mesoporous Mater. 309, 110573.

Ossman, M.E., Mansour, M.S., Fattah, M.A., Taha, N., Kiros, Y., Peanut shells and talc powder for removal of hexavalent chromium from aqueous solutions. Bulg. Chem. Commun. 46, 629-639.

Pan, J.J., Jiang, J., Xu, R.K., 2014. Removal of Cr (VI) from aqueous solutions by Na_2SO_3/$FeSO_4$ combined with peanut straw biochar. Chemosphere 101, 71–76. https://doi.org/10.1016/j.chemosphere.2013.12.026.

Picard, M., Thakur, S., Misra, M., Mielewski, D.F., Mohanty, A.K., 2020. Biocarbon from peanut hulls and their green composites with biobased poly (trimethylene terephthalate)(PTT). Sci. Rep. 10, 1–14. https://doi.org/10.1038/s41598-020-59582-3.

Raj, A., Raju, K., Varghese, H.T., Granadeiro, C.M., Nogueira, H.I.S., Panicker, C.Y., 2009. IR, Raman and SERS spectra of 2-(methoxycarbonylmethylsulfanyl)-3, 5-dinitrobenzene carboxylic acid. J. Braz. Chem. Soc. 20, 549–559. https://doi.org/10.1590/S0103-50532009000300021, 2009.

Rodrigues, E., Almeida, O., Brasil, H., Moraes, D., dos Reis, M.A.L., 2019. Adsorption of chromium (VI) on hydrotalcite-hydroxyapatite material doped with carbon nanotubes: equilibrium, kinetic and thermodynamic study. Appl. Clay Sci. 172, 57–64. https://doi.org/10.1016/j.clay.2019.02.018.

Santhosh, C., Daneshvar, E., Tripathi, K.M., Baltrėnas, P., Kim, T., Baltrėnaitė, E., Bhatnagar, A., 2020. Synthesis and characterization of magnetic biochar adsorbents for the removal of Cr (VI) and Acid orange 7 dye from aqueous solution. Environ. Sci. Pollut. Res. 27, 32874–32887. https://doi.org/10.1007/s11356-020-09275-1.

Silva, T.C.F., VergÜtz, L., Pacheco, A.A., Melo, L.F., Renato, N.S., Melo, L.C.A., 2020. Characterization and Application of Magnetic Biochar for the Removal of Phosphorus from Water, vol. 92. Anais da Academia Brasileira de Ciências. https://doi.org/10.1590/0001-3765202020190440.

Tran, H.N., Van Pham, V., Vo, D.-V.N., Nguyen-Tri, P., 2019. Removal of hexavalent chromium by biochar supported nZVI composite: batch and fixed-bed column evaluations, mechanisms, and secondary contamination prevention". Chemosphere 233, 988–990. https://doi.org/10.1016/j.chemosphere.2018.11.009.

Van Tran, T., Nguyen, D.T.C., Le, H.T.N., Vo, D.-V.N., Doan, V.-D., Dinh, V.-P., Nguyen, H.-T.T., Nguyen, T.D., Bach, L.G., 2019. Amino-functionalized MIL-88B (Fe)-based porous carbon for enhanced adsorption toward ciprofloxacin pharmaceutical from aquatic solutions. C R Chim 22, 804–812. https://doi.org/10.1016/j.crci.2019.09.003.

Van Tran, T., Dai Cao, V., Nguyen, V.H., Hoang, B.N., Vo, D.-V.N., Nguyen, T.D., Bach, L. G., 2020. MIL-53 (Fe) derived magnetic porous carbon as a robust adsorbent for the removal of phenolic compounds under the optimized conditions. J. Environ. Chem. Eng. 8, 102902. https://doi.org/10.1016/j.jece.2019.102902.

World Health Organization, 2000. The World Health Report 2000: Health Systems: Improving Performance.

World Health Organization, 2011. Guidelines for Drinking-Water Quality, vol. 216, pp. 303–304.

Xu, J., Cao, Z., Zhang, Y., Yuan, Z., Lou, Z., Xu, X., Wang, X., 2018. A review of functionalized carbon nanotubes and graphene for heavy metal adsorption from water: preparation, application, and mechanism. Chemosphere 195, 351–364. https://doi.org/10.1016/j.chemosphere.2017.12.061.

Zhang, M., Gao, B., Yao, Y., Xue, Y., Inyang, M., 2012. Synthesis of porous MgO-biochar nanocomposites for removal of phosphate and nitrate from aqueous solutions. Chem. Eng. J. 210, 26–32. https://doi.org/10.1016/j.cej.2012.08.052.

Zhong, Z.Y., Yang, Q., Li, X.M., Luo, K., Liu, Y., Zeng, G.M., 2012. Preparation of peanut hull-based activated carbon by microwave-induced phosphoric acid activation and its application in Remazol Brilliant Blue R adsorption. Ind. Crop. Prod. 37, 178–185. https://doi.org/10.1016/j.indcrop.2011.12.015.